BRDF characterization of Al-coated thermoplastic polymer surfaces

Tommaso Fontanot, Jan Audenaert, Peter Hanselaer, Ilaria Pecorari, Vanni Lughi, Erik Vesselli, Sara Paroni, Frédéric B. Leloup

Abstract In this paper, we present a combined morphological and optical characterization of aluminum-coated thermoplastic polymer surfaces. Flat plastic substrates, obtained by means of an injection molding process starting from plastic granules, were coated with ultra-thin aluminum films evaporated *in vacuo*, on top of which a silicon-based protective layer was plasma deposited in order to prevent oxidation of the metal reflective surface. Different sample treatments were studied to unravel the influence of substrate chemistry, substrate thickness, aluminum and protective layer thickness, and surface roughness on the actual optical reflectance properties. Bidirectional reflectance distribution function measurements, corroborated by surface morphological information obtained by means of atomic force microscopy, correlate reflectance characteristics with the root-mean-square surface roughness, providing evidence for the role of the substrate and the thin films' morphology. The results unravel information of interest within many applicative fields involving metal coating processes of plastic substrates as an example in the case of automotive lighting.

Keywords BRDF, Aluminum coating, Thin film, AFM, Surface roughness

T. Fontanot, E. Vesselli (✉)
Department of Physics, University of Trieste, Via A. Valerio 2, 34127 Trieste, Italy
e-mail: evesselli@units.it

T. Fontanot, S. Paroni
Marelli Automotive Lighting Italy S.p.A., Via dell'Industria 17, 33028 Tolmezzo, Udine, Italy

J. Audenaert, P. Hanselaer, F. B. Leloup (✉)
Light and Lighting Laboratory, Department of Electrical Engineering (ESAT), KU Leuven, Gebroeders De Smetstraat 1, 9000 Ghent, Belgium
e-mail: Frederic.Leloup@kuleuven.be

I. Pecorari, V. Lughi
Department of Engineering and Architecture, University of Trieste, Via A. Valerio 6a, 34127 Trieste, Italy

E. Vesselli
Istituto Officina dei Materiali CNR-IOM TASC Laboratory, Area Science Park, S.S. 14 km 163.5, 34149 Trieste, Italy

Introduction

The deposition of metallic layers on different substrates has gained increasing attention in a large variety of industrial fields, such as electronics,[1] biotechnology,[2] and chemistry,[3] to mention a few examples. Metallization processes are extensively used because they enable tailoring of crucial properties such as electric conductivity,[4] adhesion,[5] corrosion resistance,[6] and thermal and optical characteristics.[7,8] The automotive industry exploits metallization processes within the framework of several applicative fields, covering a large number of components and functions.[9,10] In this paper, we examine the optical properties of metallized plastic reflector components of automotive rear lamps, which are used in combination with a light source to obtain the desired light intensity and intensity distribution. The purpose of the metallization process applied to automotive rear lamps is dual: on one side, it must provide the photometry imposed by the market regulation (functional value) while, on the other side, it represents a style feature (aesthetical value). A dedicated set of samples, which serve as prototype reflector materials in automotive rear lamps, was prepared by applying a variety of metallization treatments on different plastic substrates. Optical properties, such as total reflectance, specular reflectance, and scattering behavior, were examined at each step of the reflector

coating process by exploiting different characterization techniques. Theoretical reflectance scattering models were sought to fit and parameterize the experimental data, with the future aim of implementing the studied reflector materials in a ray-tracing simulation environment as a tool for developers in the lighting design process. Finally, we verified the possibility of extracting information about the surface roughness directly from the optical measurements, yielding results in line with parallel, direct roughness measurements performed by means of atomic force microscopy (AFM).

Materials and methods

Sample preparation

The substrates used in this study consist of black polymeric plates obtained via injection molding from plastic granules of either polycarbonate (PC) or acrylonitrile butadiene styrene (ABS). Aluminum (Al) was deposited by means of thermal physical vapor deposition (PVD) *in vacuo* (10^{-4} mbar) onto the substrates kept at room temperature.[11–14] To prevent oxidation and damage of the reflectors under standard working conditions induced by environmental factors, hexamethyldisiloxane (HMDSO) silicon-based protective layer was plasma deposited over the reflective Al film, yielding a hetero-stacked material. In the end, a set consisting of 40 different samples was prepared with the aforementioned approach to investigate the role of several parameters, including the substrate material (PC or ABS), its thickness (1.5 or 3 mm), and the thickness of the Al film and of the protective layer. (A schematic representation of the sample heterostacks is shown in Fig. 1a.)

Optical characterization

The bidirectional reflectance distribution function (BRDF) was measured to evaluate the optical reflection properties of each sample. Theoretically, the BRDF describes the spectral reflectance properties of a material at any angle of illumination or viewing. The introduction of the concept and notation of the BRDF is accredited to Nicodemus et al.[15] Along a selected viewing direction, the BRDF is defined in radiometric terms as the surface radiance of a sample due to the scattering of the incident radiation from a defined direction of irradiation:

$$q_{e,\lambda}(\theta_i, \varphi_i, \theta_s, \varphi_s, \lambda) = \frac{\mathrm{d}L_{e,\lambda,s}(\theta_i, \varphi_i, \theta_s, \varphi_s, \lambda)}{\mathrm{d}E_{e,\lambda,i}(\theta_i, \varphi_i, \lambda)} \left[sr^{-1}\right],$$

$q_{e,\lambda}$ being the spectral BRDF, (θ_i, φ_i) the polar and azimuthal angles of the impinging light beam, (θ_s, φ_s) the polar and azimuthal angles of the scattered light, $\mathrm{d}L_{e,\lambda,s}$ the differential spectral radiance, and $\mathrm{d}E_{e,\lambda,i}$ the differential spectral irradiance from an infinitesimal solid angle. The angular coordinates refer to the surface normal. A home-built full three-dimensional BRDF instrument (see Fig. 1) was used to measure the BRDF of the different samples. The light source in the illumination section (Fig. 1b) consists of a xenon arc lamp mounted in a lamp housing, in front of which a diaphragm is positioned; an image of the diaphragm aperture is formed at the detector plane by use of a collimating mirror. The detection section (Fig. 1c) includes a collector lens, imaging the sample area onto an aperture of an integrating cavity, which in turn is

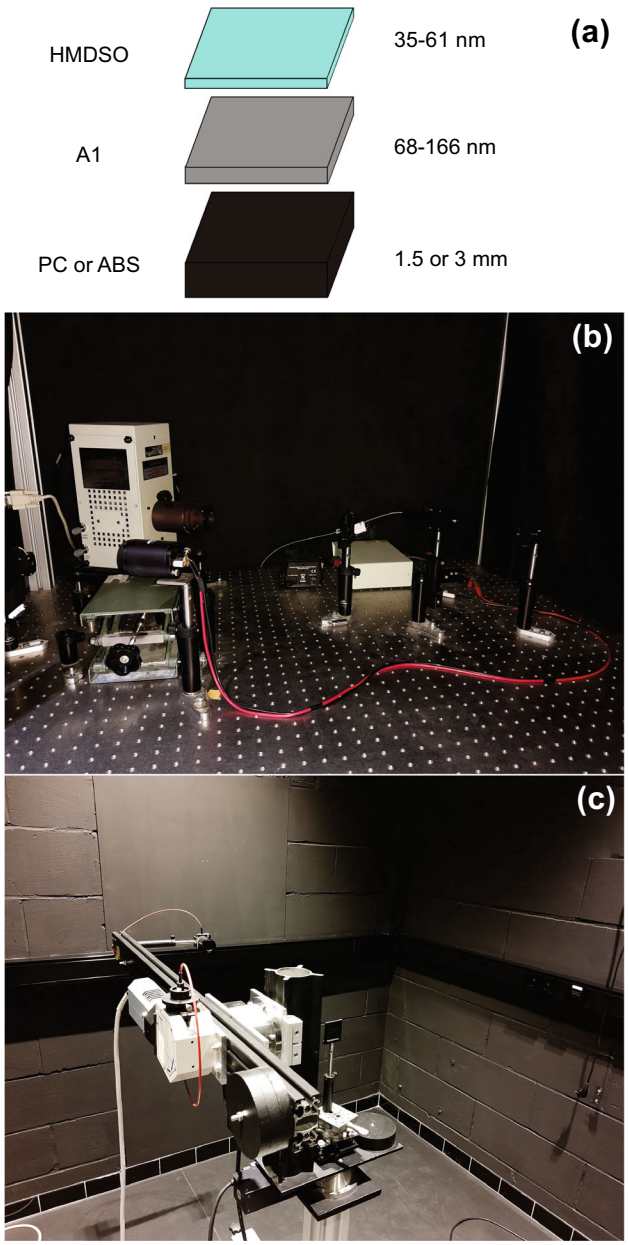

Fig. 1: (a) Schematic representation of the sample compositions and BRDF measurement setup showing (b) the illumination section and (c) the detection section

coupled to a spectrometer with interchangeable gratings, by use of a high-grade fused silica fiber bundle. The detector head is mounted on a bench, which can be rotated by aid of two motorized rotation stages, enabling alignment at any viewing angle with respect to the sample. The sample holder allows manual positioning and alignment of the specimen by adjusting two rotation stages and one translation stage. For a more detailed description of the instrument, we refer to Leloup et al.[16]

All BRDF measurements were performed at an incident angle of 45°. In particular, the 45°, 0°: 45°, 180° geometry was used for the wavelength dependence measurements, while the 45°, 0°: x, 180° geometry—with x in the interval [20°, 70°]—was adopted for the angular dependence investigations.[17] The integration time was optimized for each viewing angle. All measurements were dark current corrected.

Atomic force microscopy (AFM)

AFM is a surface scanning probe technique, yielding morphological and chemical information at surfaces with atomic-scale lateral resolution.[18] Here, an AFM Solver Pro-M (NT-MDT, Russia) was used to characterize the films in terms of thickness and surface roughness. The AFM was equipped with a NSG01 tetrahedral Si tip with nominal resonance frequency in the 87–230 kHz range. By opportunely choosing among the possible instrument working modes (contact, noncontact, and tapping), the microscope was operated in tapping mode and all measurements were carried out in air at room temperature. The tapping mode was preferred over other contact and noncontact approaches since it allows better lateral resolution, while still preserving the surface from damage.

Results and discussion

AFM characterization

In order to measure the thickness of the Al and HMDSO coatings, a photoresist mask (S1818 G2 from ''Rohm and Haas'', Denmark) was pre-deposited on the substrate via photolithography before the evaporation of the respective coatings. After spin coating and hot plating, a mask with a precise geometric pattern was used to generate a sharp step between the bare substrate and the area covered with the photoresist mask (UV radiation: 250 nm; developer bath: MF319 from ''Rohm and Haas'', UK). The samples were then metallized and, after removing the photoresist with a lift off process in acetone, a sharp step between the metallized and nonmetallized (previously protected) regions was obtained (example shown in Fig. 2). The film and coatings thickness was then obtained by measuring the step height.[19]

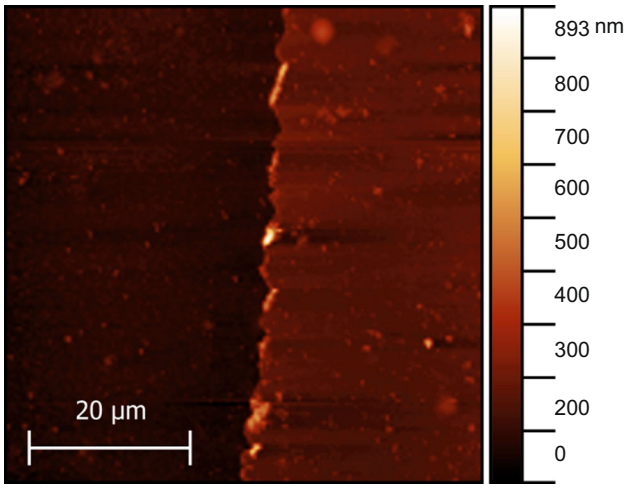

Fig. 2: Selected AFM image acquired over the step. The height difference between the bare surface (left) and the metal film (right) provides a measurement of the Al layer thickness. The topographic quantitative height profile of the image is color-coded (scale on the right)

Four different Al deposition recipes were tested, resulting in different Al-layer thickness values of (68 ± 3) nm, (81 ± 3) nm, (115 ± 7) nm, and (166 ± 3) nm, respectively. The uncertainties represent the statistical error originating from multiple measurements performed along the step edge. Two HMDSO evaporation recipes were also tested, yielding (35 ± 4)-nm and (61 ± 1)-nm-thick protective layers. From the AFM images, the surface roughness is calculated as the root-mean-square (rms) (σ)

$$\sigma = \sqrt{\frac{1}{n}\sum_{i=1}^{n} y_i^2}$$

where y_i is the difference between every local height with respect to the average height of the region taken into account (Fig. 3).

Both the actual roughness values and the associated uncertainties were obtained statistically, i.e., by collecting and averaging local information from several regions on each sample (sampling window kept at a constant size of 20 × 20 µm^2). In particular, the central part (150 × 150 pixels) of each full-size image (256 × 256 pixels) was taken into account, excluding the external frame to avoid border and drift effects. The central region was divided into nine subregions (50 × 50 pixels, around 4 × 4 µm^2 each); mean values and standard deviations have been obtained performing the analysis on these nine subregions (results are reported in Table 1). The rms surface roughness value for PC-based samples was found to be on the order of 5 nm, whereas ABS-supported films exhibited a higher surface roughness (20–30 nm). Taken together, these data show a predominant influence of the substrate on the rms surface roughness, rather than of the coating

thickness. A detailed discussion is presented in the ''Results and discussion'' section, where a comparison with the rms surface roughness values obtained from the BRDF measurements is considered.

Role of the substrate

Since the rms surface roughness seemed to be primarily determined by the type of substrate (PC vs. ABS), a first issue that was investigated was the role of the substrate on surface reflectance. The spectral BRDF of coated PC and ABS samples of 1.5 and 3-mm-thickness was therefore measured (Fig. 4). In the selected case shown in the figure, the thickness of the Al and protective coatings was the same for all samples, i.e., (115 ± 7) nm and (35 ± 4) nm, respectively (AFM data). This specific configuration was selected because it best represents what is implemented at the applicative industrial level.

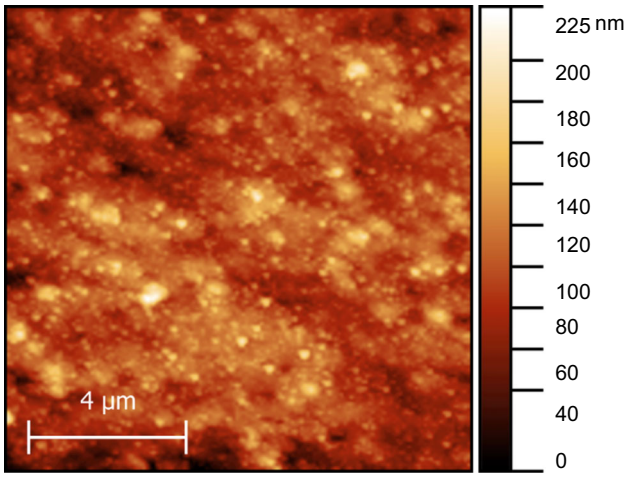

Fig. 3: Selected AFM image of an Al-coated 3 mm ABS substrate. The figure is representative of the samples studied by means of AFM, putting in evidence the characteristic the surface inhomogeneity

The spectral BRDF, measured in the 45°, 0°: 45°, 180° geometry, is shown in Fig. 4a. Major differences in the scattering properties of the two sample types can be noticed readily at a first glance. The trend is very different for the two types of substrates: for PC, the spectral BRDF slightly increases with wavelength (10%) for both the 1.5 mm (3874 and 4209 sr^{-1}) and the 3 mm (4348 and 4740 sr^{-1}) thick substrates, while for ABS, this wavelength-dependence is more pronounced (35%) for the two thickness values (1.5 mm: 2372 and 3503 sr^{-1}; 3 mm: 2669 and 3918 sr^{-1}). The angular distribution of the BRDF, measured in the 45°, 0°: x, 180° geometry with x in the interval [20°, 70°] at a wavelength of 555 nm, is depicted in Fig. 4b (angles refer to the sample surface normal). PC samples show a narrower specular distribution than ABS samples, corresponding to a greater capacity of PC to act as a mirror-like material. For both sample types, the BRDF increases with substrate thickness. Indeed, for the ABS samples, the specular BRDF peak at 555 nm for the 3 mm specimen is significantly higher than the value of the 1.5 mm specimen (approximately 9% difference, 3590 sr^{-1} vs. 3307 sr^{-1}, respectively), while for the PC specimens the relative difference is even larger (13%, 4703 sr^{-1} vs. 4112 sr^{-1}). This trend was found for all

Table 1: Surface roughness values extracted from BRDF, AFM, and total reflectance measurements. The surface roughness is primarily determined by the substrate type

Substrate	Substrate thickness (mm)	Al thickness (nm)	Protector thickness (nm)	BRDF rms (nm)	AFM rms (nm)	Total reflectance rms (nm)
ABS	1.5 ± 0.1	115 ± 7	35 ± 4	20 ± 3	21 ± 4	14 ± 1
ABS	3.0 ± 0.1	68 ± 3	35 ± 4	19 ± 3	26 ± 4	17 ± 2
ABS	3.0 ± 0.1	81 ± 3	35 ± 4	19 ± 3	22 ± 3	16 ± 2
ABS	3.0 ± 0.1	115 ± 7	35 ± 4	20 ± 3	30 ± 5	15 ± 2
ABS	3.0 ± 0.1	115 ± 7	0	24 ± 3	20 ± 2	17 ± 2
ABS	3.0 ± 0.1	115 ± 3	61 ± 1	22 ± 3	21 ± 2	17 ± 2
ABS	3.0 ± 0.1	166 ± 3	35 ± 4	20 ± 3	23 ± 3	17 ± 2
PC	1.5 ± 0.1	115 ± 7	35 ± 4	5 ± 1	6 ± 1	4 ± 1
PC	3.0 ± 0.1	68 ± 3	35 ± 4	5 ± 1	5 ± 1	4 ± 1
PC	3.0 ± 0.1	81 ± 3	35 ± 4	7 ± 1	8 ± 2	5 ± 1
PC	3.0 ± 0.1	115 ± 7	35 ± 4	6 ± 1	7 ± 2	4 ± 1
PC	3.0 ± 0.1	115 ± 7	0	5 ± 1	6 ± 1	4 ± 1
PC	3.0 ± 0.1	115 ± 7	61 ± 1	5 ± 1	6 ± 1	5 ± 1
PC	3.0 ± 0.1	166 ± 3	35 ± 4	4 ± 1	13 ± 2	3 ± 1
ABS	1.5 ± 0.1	0	0	12 ± 1	14 ± 3	20 ± 2
ABS	3.0 ± 0.1	0	0	14 ± 2	19 ± 4	21 ± 2
PC	1.5 ± 0.1	0	0	2 ± 1	3 ± 1	9 ± 1
PC	3.0 ± 0.1	0	0	2 ± 1	4 ± 1	9 ± 1

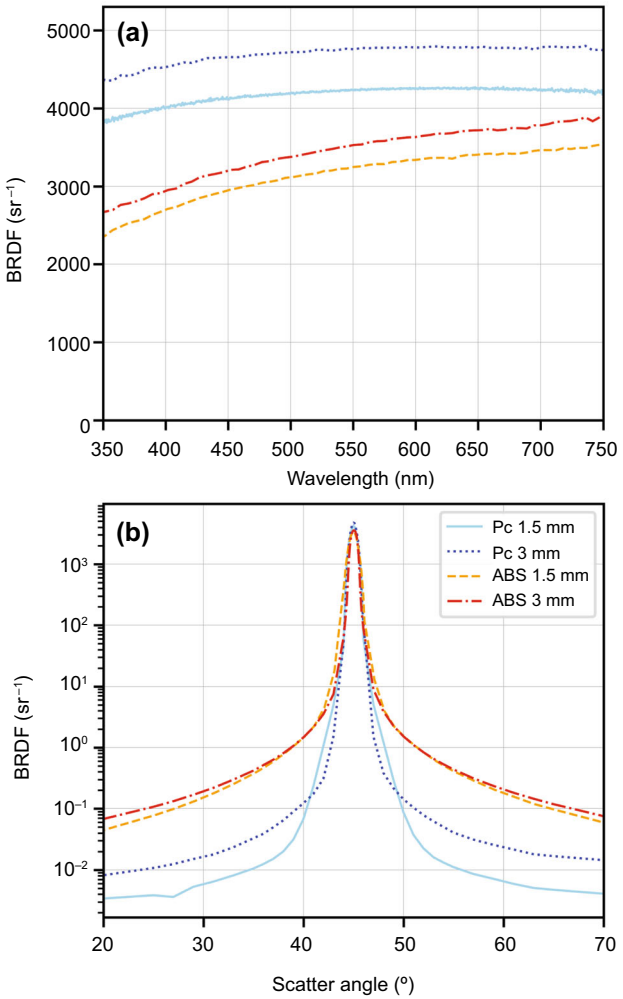

Fig. 4: BRDF for the different substrates (PC and ABS, 1.5 and 3 mm) coated with (115 ± 7) nm of Al and (35 ± 4) nm hexamethyldisiloxane; (a) spectral dependence (45°: 45° specular geometry); (b) angular (555 nm) dependence. Angles refer to the sample surface normal

samples characterized in the study, verifying the reasonable conclusion that rougher surfaces exhibit a much more diffuse behavior with respect to smoother samples. Profilometry measurements revealed that the 1.5 mm substrate displays long-range surface height deformations of about 12 μm in a 20 mm range, while for the 3 mm substrate the recorded value is an order of magnitude lower (Fig. 5). This finding confirms the BRDF data, indicating that thinner substrates undergo deformation at the injection molding production stage, thus before the coating process.

Role of the Al film

As specified in the "Methods and materials" section, both PC and ABS substrates (1.5- and 3-mm thickness) were coated with an Al layer of thickness between 70

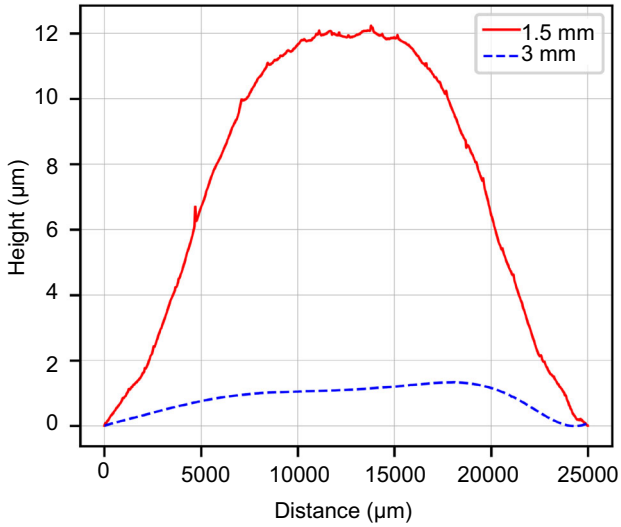

Fig. 5: Profilometer measurements on the plastic plates; 1.5 mm PC (red full line), 3 mm PC (blue dashed line). Similar results were obtained for the ABS case

and 170 nm, depending on the evaporation recipe. A (35 ± 4) nm HMDSO protective layer was post-deposited. The BRDFs of the 3 mm PC samples with an Al coating thickness of (68 ± 3) nm, (81 ± 3) nm, (115 ± 7) nm, and (166 ± 3) nm, respectively, are shown in Fig. 6. The BRDF data of a 3-mm-thick bare PC sample is also shown for direct comparison (cyan full line). As expected, the addition of the Al layer increases the BRDF value by about one order of magnitude, both in the specular and off-specular directions. Interestingly, the Al-layer film thickness does not seem to affect the BRDF peak value, apart from the case of the thickest film (166 nm), which yields a significantly lower BRDF intensity.

As for the spectral dependence of the BRDF, measured in the 45°, 0°: 45°, 180° geometry (Fig. 6a), it is observed that the overall shape of the function is similar for all Al films, showing increasing reflectance with wavelength. Clear differences are observed for what concerns the angular dependence of the BRDF (Fig. 6b), indicating best specular and off-specular reflectance for an Al layer thickness between 81 and 115 nm. The total reflectance of the samples was measured by means of a HunterLab Ultrascan PRO spectrophotometer (8°: *d* geometry). In particular, we found that the total reflectance (specular included) amounts to (82 ± 2) % for Al thickness in the range of 68–115 nm, slightly decreasing to (79 ± 1) % for the 166 nm Al film, in contrast with only (5 ± 1) % for the bare PC substrate. Near similar conclusions are drawn from the results obtained for the thinner (1.5 mm) PC substrate, apart from the effects ascribed to the substrate deformation, as discussed above. Upon changing material (from PC to ABS), the Al-covered 3-mm-thick ABS samples again yield an almost one order of magnitude higher BRDF than the bare ABS surface (Figs. 7a and 7b). Regarding the spectral

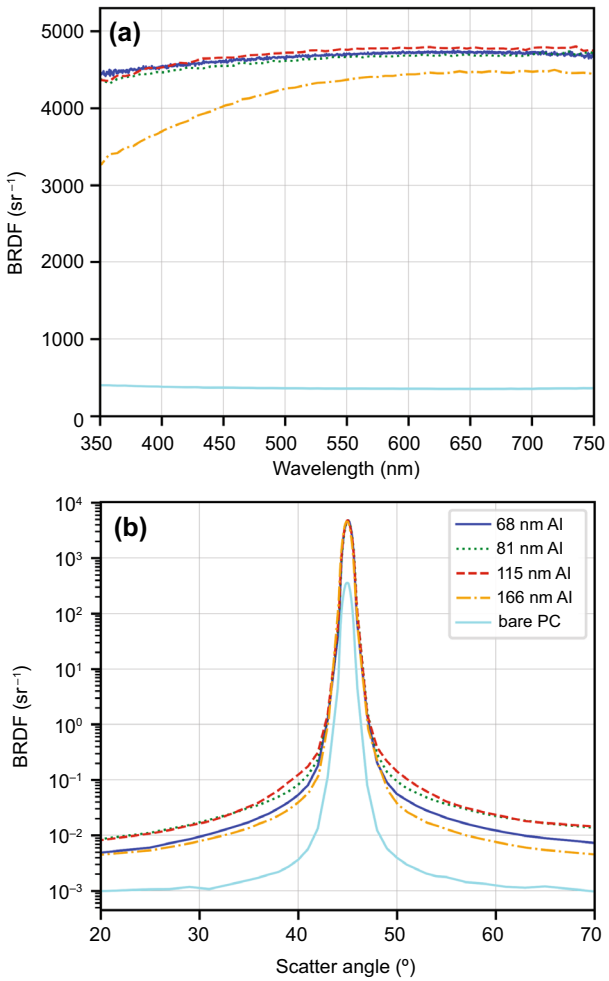

Fig. 6: Dependence of the BRDF on the Al film thickness for a 3 mm PC substrate; (a) spectral (45° with respect to the sample surface normal) and (b) angular (555 nm) BRDF. The Al thickness values reported in the figure are: 68 nm (blue continuous line), 81 nm (green dotted line), 115 nm (red dashed line), 166 nm (orange dot-dashed line) and bare PC (continuous cyan line). Apart from the bare PC, all samples have a 35 nm HMDSO protective layer

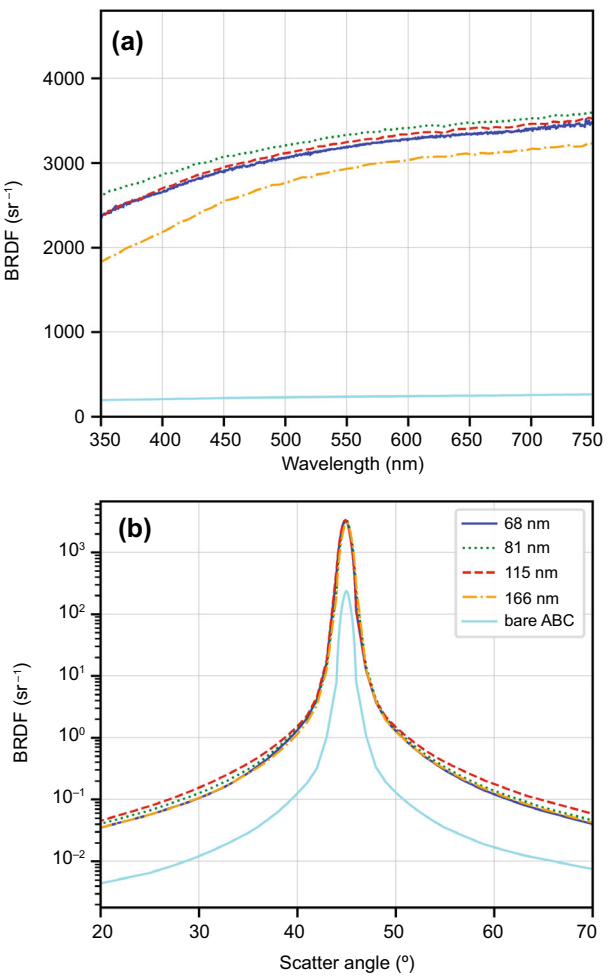

Fig. 7: Dependence of the BRDF from the Al film thickness for a 3 mm ABS substrate; (a) spectral (45° with respect to the sample surface normal) and (b) angular (555 nm) BRDF. The Al thickness values reported in the figure are: 68 nm (blue continuous line), 81 nm (green dotted line), 115 nm (red dashed line), 166 nm (orange dot-dashed line) and bare ABS (continuous cyan line). Apart from the bare ABS, all samples have a 35 nm HMDSO protective layer

distribution (Fig. 7a), the ABS sample with an 81-nm-thick Al film yields the highest signal, while the lowest BRDF is observed for the thickest coating (166 nm Al), in analogy with the PC case. The spectral trend is also similar, yielding progressively increasing BRDF values for increasing wavelength. Concerning the BRDF angular dependence (Fig. 7b), similar to the PC case, the highest BRDF can be obtained with a coating thickness ranging between 81 and 115 nm. The total reflectance ranges from (70 ± 1) % to (69 ± 1) % for the samples characterized by 68, 81, and 115 nm Al layer, respectively, while it drops to (66 ± 1) % for the 166 nm Al sample. For the bare ABS substrate, the total reflectance is (5 ± 1) %.

Therefore, it is found that for both ABS and PC substrates, the Al coating thickness yielding best spectral and spatial (both in the specular and off-specular directions) properties ranges between 81 and 115 nm, corresponding to best integrated reflectance.

Role of the protective layer

As mentioned above, the HMDSO protective layer is plasma deposited over the Al film in order to prevent both oxidation and mechanical damage. The influence of this necessary protection on the surface scattering properties was analyzed for six different types of samples. Different HMDSO evaporation recipes were adopted, yielding HMDSO films of (35 ± 4) and (61 ± 1) nm as quantified by means of AFM, respectively, on top of both PC and ABS substrates covered by a (115 ± 7)-nm-thick Al film. A bare Al film without protective layer was adopted as a reference.

The measured spectral BRDF in the 45°, 0°: 45°, 180° geometry and the spatial distribution at 555 nm for the 3-mm-thick PC substrates is depicted in Figs. 8a and 8b. The total reflectance measured with the HunterLab spectrophotometer amounts to (85 ± 1) %, referred to the sample without protective layer on top, (82 ± 1) % for the specimen with the 35-nm-thick protective layer, and (76 ± 1) % for the specimen with the 61-nm-thick protective layer.

As expected, the protective layer affects the spatial BRDF. The BRDF peak at 555 nm drops from 4732 sr^{-1} for the uncoated film to 4246 and 3340 sr^{-1} for the samples covered by 35 and 61 nm of HMDSO, respectively. Interestingly, a 35-nm-thick protective layer yields the lowest signal for angles far from the specular direction, while a thicker coating (61 nm) introduces a broader angular dispersion. Summarizing, the protective layer deposited on the Al film supported by PC hampers the reflectance in the specular direction, while it introduces an angular spreading.

Data for the ABS substrates metallized with 115 nm of Al and covered with different HMDSO films are shown in Fig. 9. The bare Al film displays the largest BRDF peak value at all wavelengths (Fig. 9a) while, at variance with the PC samples case, the sample with an intermediate protector layer thickness (35 nm) has the lowest specular reflectance. Remarkably, the thickest protective layer (61 nm) behaves like the bare aluminum at wavelengths below 430 nm, drastically changing its trend for wavelengths greater than 430 nm, resembling the 35 nm HMDSO sample profile. This is ascribed to the role of the CH species in HMDSO, which is known to contribute with transition lines at a wavelength of 430 nm.[20,21] The contribution of the CH species is also observed on PC substrates (Fig. 8a), starting from 430 nm in the spectrum from the 61 nm HMDSO covered sample. The different

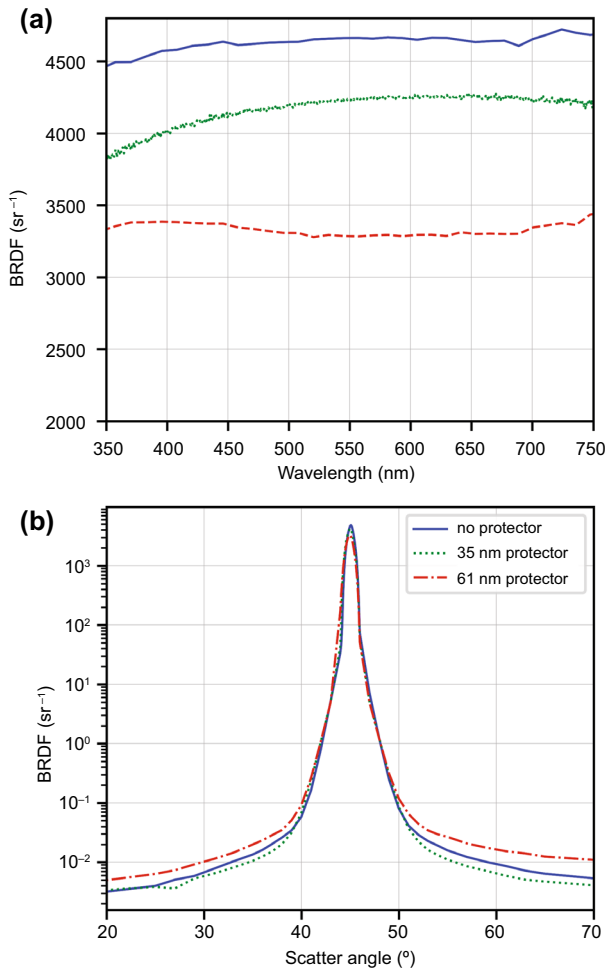

Fig. 8: Dependence of the BRDF from the thickness of the protective layer deposited on 115 nm Al on 3 mm PC; (a) spectral (45° with respect to the sample surface normal) and (b) angular (555 nm) BRDF for samples with 0-, (35 ± 4)-, and (61 ± 1)-nm-thick protective layer on top of a 115-nm-thick Al (blue continuous line, green dotted line, and red dashed line, respectively)

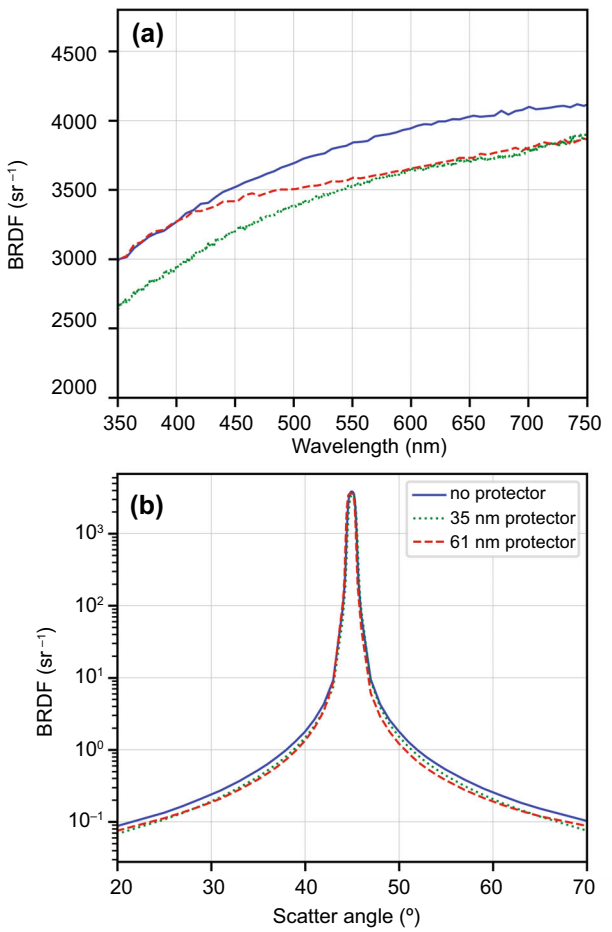

Fig. 9: Dependence of the BRDF from the thickness of the protective layer deposited on 115 nm Al on 3 mm ABS; (a) spectral (45° with respect to the sample surface normal) and (b) angular (555 nm) BRDF for samples with 0-, (35 ± 4)-, and (61 ± 1)-nm-thick protective layer on top of a 115-nm-thick Al film (blue continuous line, green dotted line, and red dashed line, respectively)

behavior in the two cases is ascribed to the diverse interaction with the substrates. The angular spread is weakly affected, as all three samples exhibit very similar properties (Fig. 9b). The total reflectance values range from (70 ± 1) % to (65 ± 1) % (the higher the HMDSO thickness, the lower the reflectance).

Quantitative analysis

The sample preparation process, described in the "Methods and materials" section, yields surfaces with isotropic roughness, as demonstrated by AFM. Moreover, it became obvious from the BRDF data that incident light is reflected within a narrow scattering angle, which brings us to compare the samples with perfect mirrors. These two observations lead us to employ the empirical *ABg* model, which is widely used in many fields,[22,23] to fit the BRDF data.[24] To analyze the specimens with the *ABg* model, we switched to the Harvey Shack representation; the most important coordinate in this reference system is $|\beta - \beta_0|$, which is the difference between the projection of the scattered beam ($\beta = \sin\theta_{\text{scatter}}$) and the projection of the specular direction ($\beta_0 = \sin\theta_{\text{specular}}$) in the plane of incidence. The *ABg* formula to fit the data is defined as

$$\text{BRDF} = \frac{A}{B + |\beta - \beta_0|^g}$$

where the parameters (A, B, and g) used in this model come from a rearrangement of the Harvey fitting function.[25] The BRDF spectra, taken at a fixed wavelength of 555 nm, have been plotted in a log–log graph with respect to ($\beta - \beta_0$). As already discussed, the substrates show small geometric deformations due to the molding process of the supports. This, combined with the finite size of the probe light beam (diameter = 1.2 cm) and with the aperture size of the detector (diameter = 1.5 cm), results in a region in which specular reflections cannot be distinguished from small angle scattered beams.[26] For the model fitting procedure, our interest is focused on the off-specular component of the reflected beam (i.e., pure scattering process component). In order to properly select the region of interest, a scan of the incident beam has been performed. This defines the angular region that must be excluded during the fitting of the model. An example of the data fitting to the *ABg* model is shown in Fig. 10, putting in evidence that only the scattered light region is taken into account (i.e., specular reflection data are excluded).

Quantitative information on the morphological properties can be obtained from the empirical *ABg* model parameters. In particular, the reconstruction of the BRDF function is attained by exploiting the fitted parameters. Integration over the space yields the total integrated scattering (TIS), defined as:

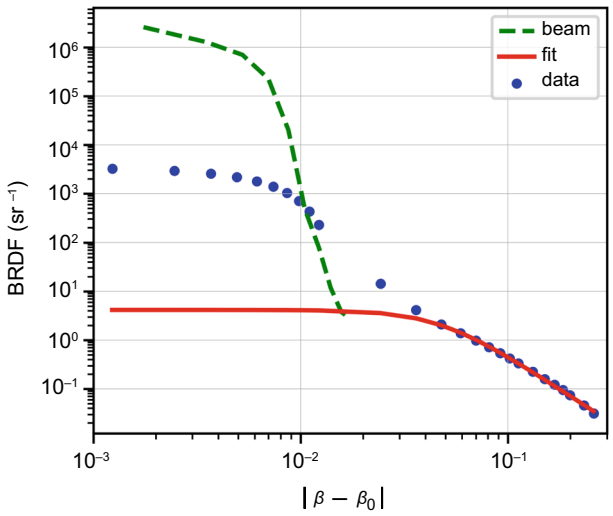

Fig. 10: Harvey Shack representation of the BRDF data (blue dots), together with the best fit according to the *ABg* model (red full line); the green dashed line represents the measured incident beam, i.e., the angular region affected by the finite size of both the light beam and detector aperture size

$$\text{TIS} = \int_{\varphi_s=0}^{2\pi} \int_{\theta_s=0}^{\pi/2} \text{BRDF}(\theta_i, \varphi_i, \theta_s, \varphi_s, \lambda) \sin\theta_s \cos\theta_s \mathrm{d}\theta_s \mathrm{d}\varphi_s$$

In our case, we calculated the TIS integral by substituting the *ABg* expression for the BRDF and operating a simple change of variable by expressing $|\beta - \beta_0|$ in terms of θ_i, θ_s, φ_s, yielding

$$\text{TIS} = \int_{\varphi_s=0}^{2\pi} \int_{\theta_s=0}^{\pi/2} \frac{A}{B + \left[(\sin\theta_s \cdot \sin\varphi_s)^2 + (\sin\theta_s \cdot \cos\theta_s - \sin\theta_i)^2\right]^{g/2}} \sin\theta_s \cos\theta_s d\theta_s d\varphi_s$$

where integration is performed on the solid angle excluding the reflection cone. In our case, the wavelength of the incident light is greater than the root-mean-square surface roughness ($\lambda >$ rms), which, as shown by our AFM measurements, is isotropic. These conditions fulfill the requirements to obtain the surface roughness (σ) from the TIS as

$$\text{TIS} = 1 - \mathrm{e}^{-\left(\frac{4\pi\cos\theta_i \sigma}{\lambda}\right)^2}$$

where θ_i is the incident beam angle with respect to the normal of the sample, and λ is the wavelength of the incident light.[27] We compared the roughness values obtained from the BRDF measurements with the corresponding values coming from the AFM experiments and from the total reflectance measurements, yielding remarkable agreement (Table 1 and Fig. 11).

Best agreement is observed between the rms values extracted from BRDF and AFM measurements, while deviations are observed for the spectrophotometer approach. This is ascribed in our case to the different angle of incidence of the light adopted for the BRDF and for spectrophotometer measurements (45° and 8°, respectively), together with the long-range deformation of the substrate (stressed in Fig. 5). Interestingly, the surface roughness results indicate that no influence is induced by increasing the film thickness of both the Al and HMDSO layers, while the main contribution comes from the polymer type used as a substrate. Specifically, the roughness values obtained on ABS-based samples are always larger than those of the corresponding PC-based heterostacks.

It has been shown that it is therefore possible to determine the surface roughness of the samples by means of a BRDF analysis based on the *ABg* model.

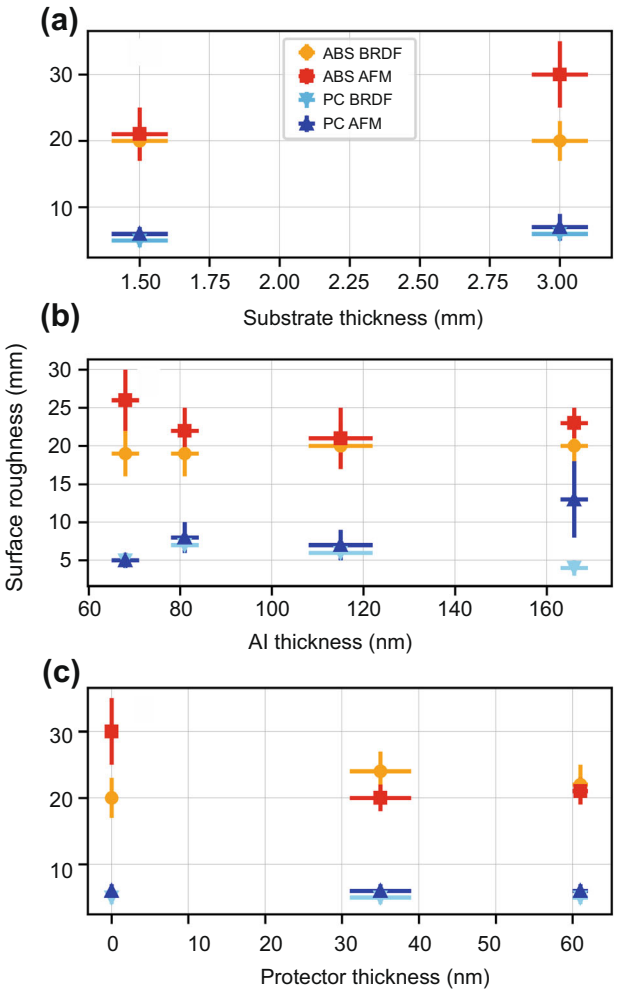

Fig. 11: Root-mean-square surface roughness extracted from AFM and BRDF measurements for samples prepared on different substrates (PC and ABS): in panel (a), the substrate thickness dependence is represented, in panel (b) the influence of the Al film thickness is showed, while in panel (c) the influence of the HMDSO film thickness is highlighted

Concerning the trends, as reasonably expected, the higher the surface roughness, the lower the specular and the higher the off-specular BRDF values. When, as stated before, this information is associated with the fact that the roughness is mainly influenced by the substrate type and not by the different metallization treatments (Fig. 11), we conclude that films supported by ABS act more as diffusers, while PC-based films behave more mirror-like. The selection of the substrate material has to be done according to the scope of the reflector: if the purpose of the reflective component is to spatially spread the light over a wider angular interval, an ABS substrate could be envisaged. If the main goal of the reflector is to focus light in a selected direction, PC should be put forward. Optimal values for the metallic film thickness were determined to maximize the total integrated reflectance (81–115 nm Al). For a thickness around 68 nm, the transmission through the Al film affects the reflectance,[28] while for thicker films the accumulation of contaminants in the deposition process may start to play a role, thus decreasing the overall reflectance.[29,30] Concerning the HMDSO, its presence is mandatory to prevent the sample from oxidation, even if it hampers the optical properties of the metal, as shown in the literature.[31] The 35 nm film performs better than the 61 nm one, while still being sufficient for adequate protection, which has been confirmed by internal validation tests performed inside the company.

Conclusions

In this paper, we have gained deeper insight into the optical properties of Al-coated thermoplastic polymer surfaces. We found that the bare ABS substrate is rougher than the PC one and observed that the actual surface roughness of the multilayer coating is dominated by the substrate material. Consequently, metallic films grown on ABS act more as diffusers, while PC substrates yield mirror-like characteristics. In an applicative view, these differences already play a relevant role in the choice of the proper substrate material for each element of the reflective part of a car head or rear lamp. As a function of the different metallization layers, the BRDF analysis revealed small spectral and angular distribution differences, so we have been able to optimize the metallization process parameters. More specifically, an Al coating of 80–115 nm optimizes the surface reflectance. Regarding the protective HMDSO layer, a 35-nm-thick film proved to be the best solution to achieve the desired optical properties and, simultaneously, prevents both surface oxidation and possible mechanical damage. Thicker coatings reduce the reflectance, affecting the optical performance of the device. The BRDF and total reflectance analysis performed within the *ABg* framework provided the retrieval of quantitative parameters that will allow modeling of the multilayer

films in a simulation software to design and engineer automotive lighting devices. The advantages of the BRDF measurements over the total reflectance approach consist of a more detailed geometrical description of the off-specular scattered components of beam, which turns out to be a key factor for the ray-tracer simulations. As a perspective, the main message to deliver is that the major role in light reflectance and scattering of polymer-supported metallic films seems to be played by the support composition and morphology, rather than by the coating process or properties.

Acknowledgments TF, IP, VL, and EV acknowledge financial support from UniTs and Marelli Automotive Lighting Italy through the project ''Caratterizzazione sperimentale e/o numerica delle proprietà ottiche ed elettroniche di materiali da impiegare per la generazione e la focalizzazione di fasci di luce con lo scopo di sviluppare nuovi sistemi ottici per il settore automotive''.

References

1. Carraro, C, Maboudian, R, Magagnin, L, ''Metallization and Nanostructuring of Semiconductor Surfaces by Galvanic Displacement Processes.'' *Surf. Sci. Rep.*, **62** 499–525 (2007)
2. Richter, J, Seidel, R, Kirsch, R, Mertig, M, Pompe, W, Plaschke, J, Schackert, HK, ''Nanoscale Palladium Metallization of DNA.'' *Adv. Mater.*, **12** 507–510 (2000)
3. Parbukov, AN, Beklemyshev, VI, Gontar, VM, Makhonin, II, Gavrilov, SA, Bayliss, SC, ''The Production of a Novel Stain-Etched Porous Silicon, Metallization of the Porous Surface and Application in Hydrocarbon Sensors.'' *Mater. Sci. Eng. C. Mater. Biol. Appl. C*, **15** 121–123 (2001)
4. Josell, D, Burkhard, C, Li, Y, Cheng, YW, Keller, RR, Witt, CA, Kelley, DR, Bonevich, JE, Baker, BC, Moffat, TP, ''Electrical Properties of Superfilled Sub-micrometer Silver Metallizations.'' *J. Appl. Phys.*, **96** 759–768 (2004)
5. Sharma, RK, Geyer, HJ, Mitchell, DG, ''Metallization Scheme Providing Adhesion and Barrier Properties.'' US Patent 4,927,505, 1990
6. Papavinasam, S, Attard, M, Arseneult, B, Revie, RW, ''State-of-the-Art of Thermal Spray Coatings for Corrosion Protection.'' *Corr. Rev.*, **26** 105–145 (2008)
7. Kim, HC, Alford, TL, ''Improvement of the Thermal Stability of Silver Metallization.'' *J. Appl. Phys.*, **94** 5393–5395 (2003)
8. Wu, Z, Wu, D, Qi, S, Zhang, T, Jin, R, ''Preparation of Surface Conductive and Highly Reflective Silvered Polyimide Films by Surface Modification and In Situ Self-metallization Technique.'' *Thin Solid Films*, **493** 179–184 (2005)
9. Hao, Y, Sim, PC, Toner, B, Frank, M, Ackermann, M, Tan, A, Kuniss, U, Kho, E, Doblaski, J, Hee, EG, Hoelke, A, Wada, S, Oshima, T, Liew, M, ''A 0.18 μm SOI BCD Technology for Automotive Application.'' 27th International Symposium on Power Semiconductor Devices & IC's (ISPSD), Hong Kong, May 2015
10. Kilian, A, Schmidt, LP, ''A Novel Fabrication Process for Printed Antennas Integrated in Polymer Multi-layer Car Body Panels.'' 2009 European Microwave Conference (EuMC), Rome, September 2009
11. Mattox, DM, *Handbook of Physical Vapor Deposition (PVD) Processing*. William Andrew, Burlington (2010)
12. Wang, J, Huang, H, Kesapragada, SV, Gall, D, ''Growth of Y-Shaped Nanorods Through Physical Vapor Deposition.'' *Nano Lett.*, **5** 2505–2508 (2005)
13. Richter, G, Hillerich, K, Gianola, DS, Monig, R, Kraft, O, Volkert, CA, ''Ultrahigh Strength Single Crystalline Nanowhiskers Grown by Physical Vapor Deposition.'' *Nano Lett.*, **9** 3048–3052 (2009)
14. Sproul, WD, ''Physical Vapor Deposition Tool Coatings.'' *Surf. Coat. Technol.*, **81** 1–7 (1996)
15. Nicodemus, FE, Richmond, JC, Hsia, JJ, ''Geometrical Considerations and Nomenclature for Reflectance.'' US Department of Commerce, National Bureau of Standards, 160 (1977)
16. Leloup, FB, Forment, S, Dutré, P, Pointer, MR, Hanselaer, P, ''Design of an Instrument for Measuring the Spectral Bidirectional Scatter Distribution Function.'' *Appl. Opt.*, **47** 5454–5467 (2008)
17. ASTM E2387-19, Standard Practice for Goniometric Optical Scatter Measurements, ASTM International, West Conshohocken, PA, 2019
18. Haugstad, G, *Atomic Force Microscopy: Understanding Basic Modes and Advanced Applications*. Wiley, Hoboken (2012)
19. Nečas, D, Klapetek, P, ''Gwyddion: An Open-Source Software for SPM Data Analysis.'' *Cent. Eur. J. Phys.*, **10** 181–188 (2012)
20. Granier, A, Vervloet, M, Aumaille, K, Vallée, C, ''Optical Emission Spectra of TEOS and HMDSO Derived Plasmas Used for Thin Film Deposition.'' *Plasma Sources Sci. Technol.*, **12** 89 (2003)
21. Gosar, Ž, Kovač, J, Mozetič, M, Primc, G, Vesel, A, ''Characterization of Gaseous Plasma Sustained in Mixtures of HMDSO and O_2 in an Industrial-Scale Reactor.'' *Plasma Chem. Plasma Proc.*, **40** 25–42 (2020)
22. Bruckman, LS, Murray, MP, Richardson, S, Brown, SA, Schuetz, MA, French, RH, *Degradation of Back Surface Acrylic Mirrors: Implications for Low Concentration and Mirror Augmented Photovoltaics*. IEEE EnergyTech, Cleveland, OH (2012)
23. Bernacki, BE, Johnson, TJ, Myers, TL, Blake, TA, ''Modeling Liquid Organic Thin Films on Substrates.'' Chemical, Biological, Radiological, Nuclear, and Explosives (CBRNE) Sensing XIX. International Society for Optics and Photonics, Orlando, FL, May 2018
24. Freniere, ER, Gregory, GG, Chase, RC, ''Interactive Software for Optomechanical Modeling.'' Lens Design, Illumination, and Optomechanical Modeling, International Society for Optics and Photonics, San Diego, CA, September 1997
25. Harvey, JE, ''Light-Scattering Characteristics of Optical Surfaces.'' Stray Light Problems in Optical Systems, International Society for Optics and Photonics, Reston, VA, September 1977
26. Audenaert, J, Leloup, FB, Durinck, G, Deconinck, G, Hanselaer, P, ''Bayesian Deconvolution Method Applied to Experimental Bidirectional Transmittance Distribution Functions.'' *Meas. Sci. Technol.*, **24** 035202 (2013)
27. Harvey, JE, Choi, N, Schroeder, S, Duparré, A, ''Total Integrated Scatter from Surfaces with Arbitrary Roughness, Correlation Widths, and Incident Angles.'' *Opt. Eng.*, **51** 013402 (2012)

28. Hass, G, Hunter, WR, Tousey, R, ''Reflectance of Evaporated Aluminum in the Vacuum Ultraviolet.'' *J. Opt. Soc. Am.*, **46** 1009–1012 (1956)
29. Karoui, A, ''Aluminum Ultra Thin Film Grown by Physical Vapor Deposition for Solar Cell Electric Nanocontacts.'' *ECS Transactions*, **41** 21–28 (2011)
30. Schmauder, T, Sauer, P, Ickes G, ''New Reflectors and Reflector Coaters.'' In 57th Annual Technical Conference Proceeding of the Society of Vacuum Coaters, Chicago, IL, May 2014
31. Schmauder, T, Küper, S, Wohlfahrt, P, ''High Reflective Silver Coatings on 3D Plastic Parts for Solar Concentrators.'' In 52nd Annual Technical Conference Proceedings of SVC, Santa Clara, CA, May 2009